remote sensing

MDPI

Review

Determination of the Leaf Inclination Angle (LIA) through Field and Remote Sensing Methods: Current Status and Future Prospects

Sijia Li [1,2,*], Hongliang Fang [1,2] and Yinghui Zhang [1,2]

[1] LREIS, Institute of Geographic Sciences and Natural Resources Research, Chinese Academy of Sciences, Beijing 100101, China
[2] University of Chinese Academy of Sciences, Beijing 100049, China
* Correspondence: lisj.19b@igsnrr.ac.cn

Abstract: The leaf inclination angle (LIA), defined as the leaf or needle inclination angle to the horizontal plane, is vital in radiative transfer, precipitation interception, evapotranspiration, photosynthesis, and hydrological processes. This paper reviews the field and remote sensing methods to determine LIA. In the field, LIA is determined using direct and indirect methods. The direct methods include direct contact, photographic, and light detection and ranging (LiDAR) methods, while the indirect methods are composed of the gap fraction, four-component, and polarization measurement methods. The direct methods can obtain LIA accurately at individual leaves, crown, and plot scales, whereas the indirect methods work well for crops at the plot level. The remote sensing methods to estimate LIA are mainly based on the empirical, radiative transfer model, and gap fraction methods. More advanced inversion strategies and validation studies are necessary to improve the robustness of LIA remote sensing estimation. In future studies, automated observation systems can be developed and the LIA measurement can be incorporated into existing ground observation networks to enhance spatial coverage.

Keywords: leaf inclination angle; field measurement; remote sensing estimation; LiDAR

Citation: Li, S.; Fang, H.; Zhang, Y. Determination of the Leaf Inclination Angle (LIA) through Field and Remote Sensing Methods: Current Status and Future Prospects. *Remote Sens.* **2023**, *15*, 946. https://doi.org/10.3390/rs15040946

Academic Editor: Gabriel Senay

Received: 10 January 2023
Revised: 6 February 2023
Accepted: 7 February 2023
Published: 9 February 2023

1. Introduction

Leaf inclination angle (LIA) quantifies the inclination of the leaf or needle to the horizontal plane or the angle between the leaf surface normal and zenith (Figure 1a) [1]. LIA is formed under the comprehensive regulation of genes, hormones, and environmental factors, including light, water, temperature, and nutrition [2–4]. LIA is a key plant structural trait that determines radiative transfer [5,6], rainfall interception [7], and evapotranspiration [8], and thus affects photosynthesis and hydrological processes [4,5,9].

The probability density of LIA or the fraction of leaf area per unit LIA is expressed with the leaf angle distribution (LAD) function [10]. Theoretically, LAD can be categorized into the planophile, erectophile, extremophile, plagiophile, uniform, and spherical distributions [10]. The spherical distribution assumes that the relative probability density of the LIA is the same as the area of the corresponding sphere surface element [10]. LAD can also be described by statistical distribution functions such as the ellipsoidal distribution [11], rotated-ellipsoidal distribution [12], and two-parameter beta distribution [13]. In radiative transfer, the leaf projection function (G(θ)) is calculated as the average projection ratio of unit leaf area in the illumination or viewing direction θ [6,14]. The spherical distribution is characterized by an isotropic leaf projection function (G ≡ 0.5) [10].

LIA can be determined through field measurements and remote sensing estimation [15–19]. This paper provides a comprehensive review of the current status in the determination of LIA from the field and remote sensing methods (Sections 2 and 3). Section 4

provides future prospects concerning LIA acquisition and estimation, and Section 5 concludes the paper.

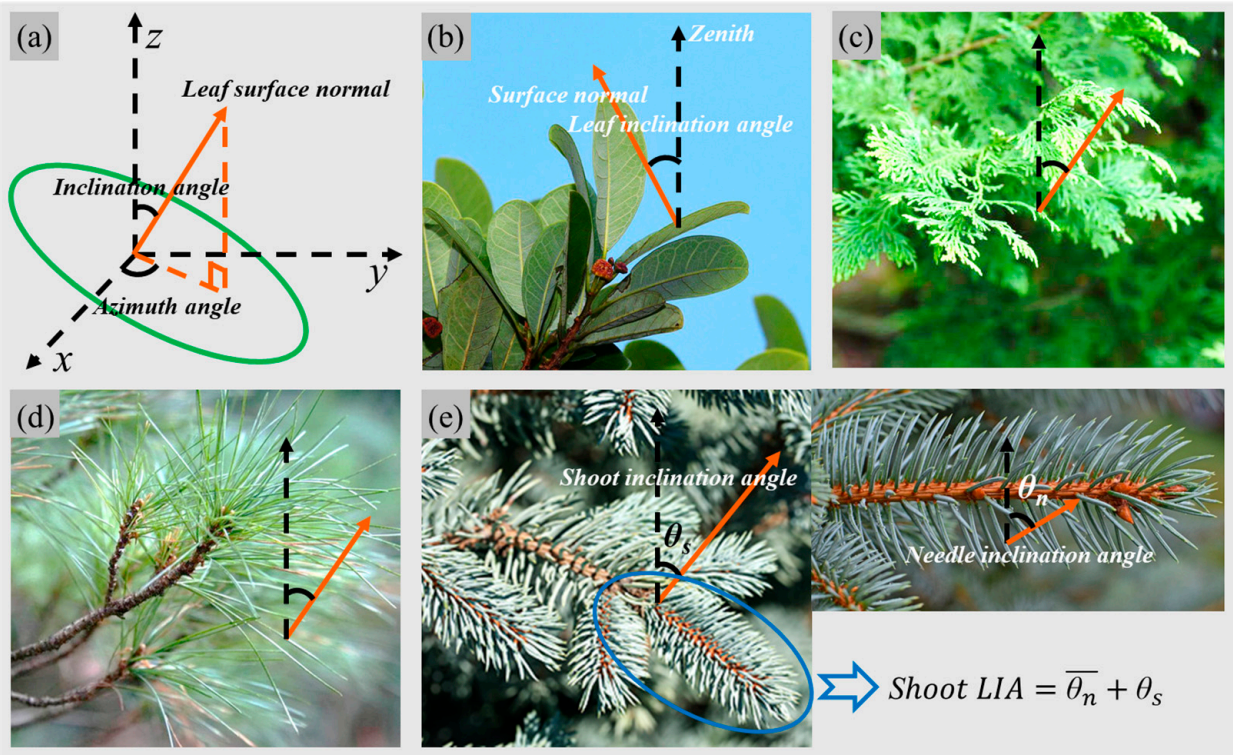

Figure 1. The schematic of leaf orientation (**a**) and the leaf inclination angle (LIA) measurement for broad leaf (**b**) and needle leaves of cypress (**c**), pine (**d**), and spruce (**e**). In (**e**), the LIA of a specified shoot is the sum of the average inclination angle for all needles within a horizontally placed representative shoot ($\overline{\theta_n}$) and the shoot inclination angle (θ_s).

2. Field Methods

2.1. Direct Methods

2.1.1. Contact Methods

Direct methods measure the actual LIA at the leaf, canopy, and plot levels from the viewpoint of the geometric structure of the leaf or needle. Among the direct methods, the contact method measures LIA manually using an inclinometer. The method has been widely used in LIA measurements of almost all biomes [15,20–22]. For flat and broad leaves, the LIA can be directly measured (Figure 1b) [15], while for long, narrow, and curved leaves, the leaf is divided into multiple segments and the LIA is the simple or area-weighted average of all segments [23]. A small difference (~6°) may exist between the two calculation methods for curved crop leaves [23]. For needleleaf trees such as the cypress, the leaf cluster can be treated as a plane and the LIA obtained as the broadleaf (Figure 1c) [24]. For pine, LIA is measured for each long needle [25] (Figure 1d). For spruce and fir, the inclination angle (θ_s) of a representative shoot is first measured and the inclination angle of all needles ($\overline{\theta_n}$) is obtained subsequently by placing the shoot horizontally. The shoot LIA is a simple sum of the two angles ($\overline{\theta_n} + \theta_s$) (Figure 1e). The canopy LIA can be calculated for all shoots with different θ_s assuming the inclination angle of all needles in each shoot ($\overline{\theta_n}$) are similar.

The 3D digitizer manually selects three or more feature points on the leaf surface and obtains their three-dimensional (3D) coordinates. The feature points are connected to a group of adjacent triangles. The normal of triangles and LIA are finally computed [26]. The 3D digitizer can be used to construct the canopy 3D model based on ray tracing to obtain the entire canopy architecture [27]. The instrument is mainly used for low or medium canopies,

particularly for crops [26,28]. However, this instrument is extremely time-consuming and cannot capture the short-term dynamic changes in the LIA (Table 1) [29,30].

The contact method is simple, accurate, and low-cost. This method directly measures the leaf angle and avoids the influence of woody materials and occlusion effect; however, the method is sometimes time-consuming, labor-intensive, and difficult to measure the plot-level LIA (Table 1). Moreover, this method is easily affected by the operator and is difficult to be used for tall forest canopies.

2.1.2. Photographic Methods

The photographic method makes non-contact LIA measurements using leveled digital photography (LDP) or stereovision. The LDP method takes horizontal photos from the canopy side, selects the leaves perpendicular to the viewing direction, and extracts the LIA using image processing software [16]. The method has been widely used for broadleaf trees and shrubs with flat leaves [16,31,32]. The method has also been extended to cereal crops with curved leaves using segmental measurement [23] and needleleaf trees [25]. Moreover, this method has been used to obtain vertical LIA of tall trees by taking photos at tower platforms (Table 1) [16]. For areas without tower platforms, the LDP method can be combined with unmanned aerial vehicles (UAV) to obtain the LIA of the entire tall canopy [33,34].

The LDP method is simple, cost-effective, and easy to perform [16,31,32]. Compared with contact methods, this method reduces field workload and possible measurement errors caused by manual contact. The non-contact characteristics of the LDP method make it easier to measure the LIA for tall canopies when there is a distance between the lifting platform and the canopy. With the LDP method, leaf and woody materials can be distinguished with visual inspection (Table 1). For canopy LIA measurement, the method assumes that the canopy leaves are uniformly distributed in azimuth and the measured LIA from one side is representative of the entire canopy [16,31]. For coniferous forests, the LDP method is appropriate for LIA measurement because the narrow shape of needles while developing automated LIA extraction algorithms is imperative. However, the method requires a lot of manual participation and is vulnerable to the influence of leaf surface curvature [35] and operator subjectivity [32]. Reliable and steady LIA can be obtained with sufficient measurements (>75) [32,36].

The methods introduced above require a lot of manual effort. The stereovision method measures single-leaf LIA automatically or semiautomatically by taking photos from different viewing angles with synchronized cameras [37–39]. The photos are processed through stereo calibration, epipolar rectification, leaf segmentation, stereo matching, and 3D reconstruction [38,40]. The method is mainly used for small- to medium-sized canopies [37,40] and is applied to monitor the diurnal variation of crop LIA [29]. Stereo pairs from smartphones were also used for obtaining LIA [41]. Recently, Yan et al. [42] used the stereovision method to measure the indoor conifer LIA based on dense matching and linear feature extraction techniques.

The stereovision method is accurate, objective, semi-automatic or automatic, and can acquire fine 3D leaf orientation. However, the method features rigorous data acquisition conditions and complex post-processing (Table 1). It is influenced by occlusion and woody materials and is difficult to use for tall canopies. The stereovision method may be integrated with UAV and advanced classification algorithms to improve its applicability.

2.1.3. LiDAR-Based Methods

Light detection and ranging (LiDAR) provides the unique capability of 3D canopy mapping and allows non-contact measurements of canopy structural attributes from terrestrial, airborne, and spaceborne platforms [43]. LIA is mainly derived from LiDAR based on dense 3D point clouds from terrestrial laser scanning (TLS) at individual canopy and plot levels [44–46]. LIA is typically obtained for crops and broad-leaved forests through the plane fitting of neighboring point clouds within a specified distance determined by

the leaf size [44,47–49]. The normal vector for each point is computed as the eigenvector corresponds to the smallest eigenvalue of the covariance matrix of neighboring points (e_2 in Figure 2b). The method has also been extended to voxel coordinates to accelerate the extraction efficiency (Figure 2c) [46]. In addition to the point and voxel LIAs [44–46], the plane fitting method was combined with a leaf clustering algorithm to extract the entire leaf LIA [50]. The entire leaf LIA can also be extracted by manually sketching 3D point clouds [51], but this practice is time-consuming and labor-intensive. To maintain sufficient point density for robust LIA measurement, multi-location scans are necessary, while single-scan TLS is not appropriate for distant canopies or tall trees (>20 m) [35].

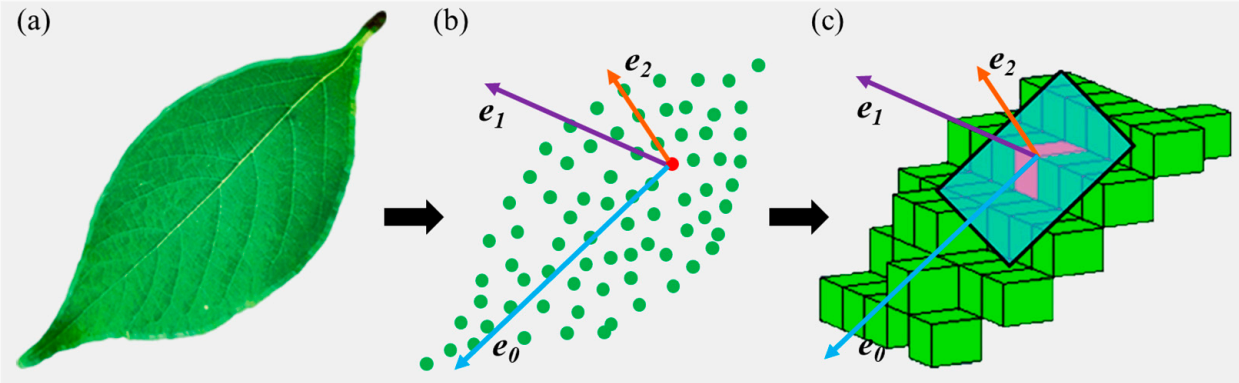

Figure 2. The LIA measurement of the leaf (**a**) based on the plane fitting of point clouds (**b**) and voxels (**c**). e_o, e_1, and e_2 denote the eigenvectors corresponding to the eigenvalues from the maximum to the minimum.

An alternative TLS method is based on the triangulation of 2D gridded point clouds [45,52] (Figure 3). The 3D point clouds (x, y, z) are projected on 2D spherical coordinates (θ, φ) encompassing zenith and azimuth angles from the TLS perspective according to the scan spaces (Figure 3a). Each point (i, j) is triangulated in the 2D gridded space by searching for and connecting neighboring hit points (Figure 3a). Once the triangulations are completed, the normal vectors of the triangles are computed in 3D space as the cross product of the two sides of the triangle, and the LIA is obtained accordingly (Figure 3c).

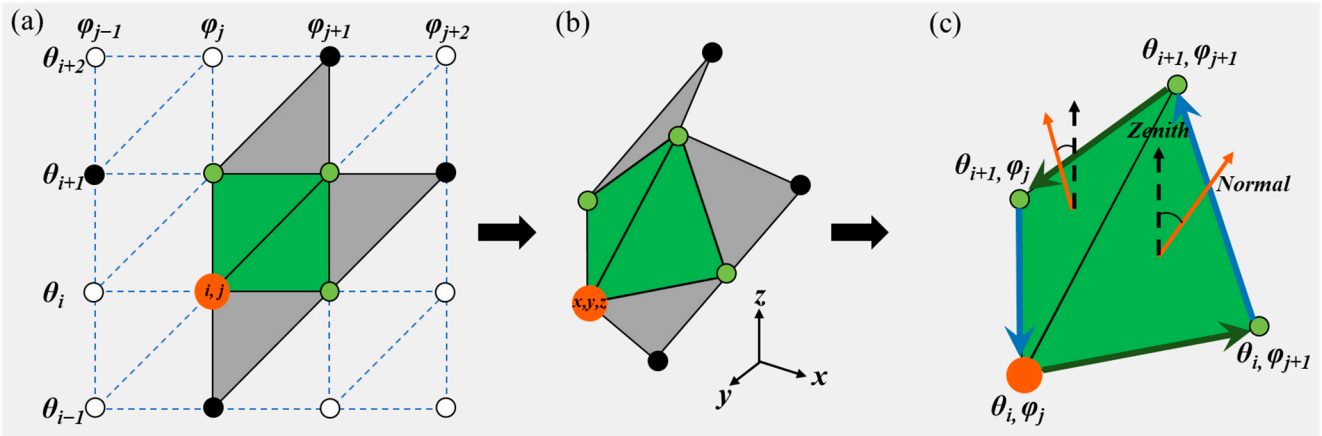

Figure 3. The schematic of point cloud triangulation in two-dimensional spherical coordinates (θ, φ) (**a**) and corresponding three-dimensional cartesian coordinates (x, y, z) (**b**). (**c**) depicts the computation of the normal vector and LIA by the cross-product of the two sides of the triangle (adapted from Bailey and Mahaffee [45]).

Airborne laser scanning (ALS) was also attempted to obtain the forest LIA based on plane fitting of neighboring points [53]. The ALS is different from TLS in the scan direction,

beam divergence, scan distance, and field of view [53]. Compared with TLS, ALS typically has a larger neighboring point distance and the laser beam size is far larger than the leaf size. Because of the lack of leaf geometric details, ALS data can only capture the inclination angles for shoot and branch, but not for individual leaves [53].

Compared with other field methods, LiDAR has prominent advantages in automatically measuring 3D leaf orientation with high accuracy and efficiency for canopies with broad and even completely curved leaves (Table 1) [35]. LiDAR typically gets different numbers of points for leaves of different sizes. In this sense, LiDAR theoretically obtains more precise LAD than other direct methods, which usually assume that LIA and the leaf area are independent and all leaf sizes are similar [16,23,31]. Few attempts have been made to estimate the LIA of needleleaf canopies because of the narrow needle size (~1 mm) [53].

LiDAR-based LIA measurements are easily biased by scan distance, scattering angle (the angle between laser beam and normal leaf vector), occlusion, woody materials, and noises (Table 1) [44,45]. The scan distance and scattering angle bias can be resolved through normal leaf weighting by the representative area of each point [45,53] or density correction [52]. The occlusion effect is largely alleviated with multiple scans or by selecting homogenous and representative subsample areas [45]. To solve the woody influence, LiDAR data can be collected during both leaf-on and leaf-off seasons for deciduous plants [50,52]. Both leaves and woody materials can also be classified separately by incorporating intensity and geometric features from point clouds [52,54,55]. In the triangulation-based method, the leaf edge effect may affect the LIA measurement [45,52]. The leaf edge effect can be solved by setting a side length threshold in the triangulation [45] or by filtering normal vectors with the scattering angle threshold [52].

2.2. Indirect Methods

2.2.1. Gap Fraction Methods

Indirect methods estimate mean leaf inclination angle (MLA) or LAD from the other variables related to LIA. One of the major variables is the angular gap fraction (GF), which denote the probability that a photo will directly penetrate the canopy in a given direction without any contact with vegetation elements [6]. Assuming that the canopy is composed of turbid mediums, the gap fraction in a given viewing direction θ ($P(\theta)$) can be described by the Beer–Lambert law [14]:

$$P(\theta) = exp^{-\frac{G(\theta)*LAI*CI(\theta)}{cos(\theta)}} \quad (1)$$

where LAI and $CI(\theta)$ represent the leaf area index and the directional clumping index, respectively. The computation of $G(\theta)$ is based on LAD, as shown below:

$$G(\theta_v) = \int_0^{\pi/2} A(\theta_v, \theta_l) g(\theta_l) d_{\theta_l} \quad (2)$$

$$A(\theta_v, \theta_l) = \begin{cases} \cos\theta_v \cos\theta_l & |\cot\theta_v \cot\theta_l| > 1 \\ \cos\theta_v \cos\theta_l \left[1 + \frac{2}{\pi}(\tan\psi - \psi)\right] & otherwise \end{cases} \quad (3)$$

$$\psi = cos^{-1}(\cot\theta_v \cot\theta_l) \quad (4)$$

where θ_v, θ_l, and ψ denote the viewing direction, normal leaf, and phase angle between the θ_v and θ_l, respectively. $g(\theta_l)$ is the probability density function of the normal leaf.

For an idealized canopy with fixed LIA and random leaf positions and azimuth angles, G(θ) shows a stable linear relationship with θ in 25–65° for each LIA [56]. MLA can thus be estimated through an empirical polynomial relationship with the slope of G(θ) acquired from the angular GFs (Equation (1)) [56]. This approach was adopted in the LAI-2200 Plant Canopy Analyzer (LI-COR Inc., Lincoln, Nebraska) (https://www.licor.com, accessed on 1 January 2023) and can be used to estimate MLA with digital hemispheric

photography (DHP) [57]. Zou, Mõttus, Tammeorg, Torres, Takala, Pisek, Mäkelä, Stoddard, and Pellikka [23] found that the cereal crop MLA obtained by LAI-2200 with the GF method was consistent with that from the manual contact measurements (R^2 = 0.92).

MLA can also be estimated through an optimization process that minimizes the cost function between the measured and simulated GFs [58]. The simulated GF is obtained (Equation (1)) by approximating the canopy LAD with the single parameter ellipsoidal distribution [11]. This method is utilized in the HemiView Forest Canopy Image Analysis System (Delta-T Devices Ltd., Cambridge, UK) (https://delta-t.co.uk/, accessed on 1 January 2023), CAN-EYE [59], and Hemisfer [60,61]. CAN-EYE uses a lookup table method to speed up the calculation efficiency, while Hemisfer considers the angular GF weights and the slope effect. The method was recently adopted by an inclined smartphone camera [62]. Zhao et al. [63] established a laser beam–vegetation hit probability model based on Equation (1) and inverted the optimal leaf projection function and its error interval from TLS data using a maximum likelihood estimator. Compared with the classical GF method, the model achieved higher accuracy and fully leveraged the raw TLS data [63].

The GF method is simple, efficient, easily conducted, and has been used by many low-cost devices (Table 1). The method can be used by LiDAR to estimate LIA, where the gap fraction can be approximated by the point cloud penetration ratio [63–65]. The method relies on turbid mediums assumption and assumes that the MLA and LAD are homogeneous and isotropic, which may be invalid in many cases [29,52,66]. When these assumptions are not met, the GF method is worse than the TLS method for heterogeneous broadleaf forests [66]. The GF estimation derived from the DHP measurement is influenced by the segment interval, image classification algorithms, illumination conditions, camera exposure, and sparkling leaves [59,67,68]. The observed GF was affected by LIA, LAI, and CI (Equation (1)), and thus, LAI and CI needed to be decoupled from the LIA estimation [69]. The GF method was unable to distinguish woody materials and was invalid for individual leaves and crowns (Table 1) [66]. The applicability of the method to coniferous forests and for acquiring vertical LIA profiles remains to be explored.

2.2.2. The Four-Component Method

The four fractions of sunlit and shaded vegetation and soil components can be classified from multi-angle images and can be linked to LAD through analytic models [69] or ray-tracing simulations [70]. Subsequently, the LAD can be estimated from the four component fractions through numerical optimization [69] or look-up table inversion technologies [70].

The four-component method fully utilizes the bidirectional fractions and can obtain reasonable LAD results at the plot level [69], while the GF method only exploits the mono-directional GFs. However, the four-component method involves a large number of parameters and may lead to an ill-posed inversion problem [70]. The method has mainly been used for simple crops but not for dense and tall vegetation canopies because of the classification difficulty and the occlusion effect (Table 1) [69,70]. The method is limited for the vertical LIA measurement and the classification procedure is influenced by the complex canopy structure, camera exposure, sky, and canopy scattering [69].

2.2.3. The Polarization Measurement

The canopy polarization reflectance primarily originates from the single scattering between photons and leaves and can be used for the LIA estimation through an empirical relationship [71]. A negative linear model was constructed to estimate the MLA from the polarized reflectance in the visible bands, particularly in the red band, and the result corresponded well with the LAI-2200 value [72]. This method is simple and efficient, and can be applied to obtain the LIA vertical profiles using portable vertical platforms. However, this method is easily affected by the solar-viewing geometry [72] and the feasibility of this method for other vegetation types, particularly coniferous forests, needs further exploration.

The direct methods measure the actual LIA based on the geometric structure of the leaf or needle, while the indirect methods estimate the MLA or LAD from gap fractions or polarization reflectance. The direct methods are typically regarded as the reference method, but are laborious for a large number of measurements [16,20,31]. The indirect methods typically estimate LIA from other variables and usually provide the MLA or LAD of the entire sample plot, but not for individual leaves or crowns [29]. In practice, the indirect methods usually obtain the plant inclination angle and may overestimate the LIA because the methods usually do not differentiate the leaves from woody materials (Table 1) [66]. The appropriate field method needs to be selected considering the vegetation types and applications.

Table 1. Comparison of different methods to obtain LIA in the field. LDP: leveled digital photography, LiDAR: light detection and ranging, GF: gap fraction method, MLA: mean leaf inclination angle, LAD: leaf inclination angle distribution.

Methods		Advantages	Disadvantages	Reference
Direct methods				
Contact		Simple, accurate, and low-cost; can be applied to leaves with different shapes and is resistant to the interference of occlusion and woody materials.	Time-consuming, labor-intensive, difficult to obtain the LIA of the tall canopy and plot-level LIA, and influenced by the operator, particularly for curved leaves.	[15,23,26,29]
Photographic	LDP	Simple, cost-effective, accurate, easily conducted, and suitable for different leaf shapes; can obtain LIA vertical profile and distinguish leaves and woody materials.	Requires a lot of manual participation, sensitive to the influence of leaf surface curvature and user subjectivity.	[16,25,31,32]
	Stereovision	Accurate, objective, semi-automatic or automatic, and can acquire fine three-dimensional leaf orientation.	Rigorous data acquisition conditions, complex post-processing, easily influenced by occlusion and woody, and difficult to measure LIA for tall canopy.	[29,37,40,42]
LiDAR		Accurate, efficient, objective, capable of capturing three-dimensional leaf orientation at leaf, crown, and plot levels, and can differentiate leaves from woody materials.	Costly, difficult data processing, not applicable to measure LIA of coniferous forests, and the LIA may be biased by heterogeneous sampling density.	[35,44,45,53]
Indirect methods				
GF		Simple, efficient, objective, low-cost, easily conducted, and can directly obtain MLA of the entire sample plot.	Sensitive to measuring conditions and post-processing, the underlying assumptions are not suitable for heterogeneous scenes, incapable of distinguishing woody materials and obtaining the LIA of individual leaves or crowns.	[29,56,58,66,73]
Four-component		Efficient, low-cost, and can directly obtain LAD of the entire sample plot.	Rigorous and enormous field measurements, tedious post-processing, not suitable for dense and tall canopy, and difficult to obtain vertical LIA and an individual leaf or crown LIA.	[69,70]
Polarization		Simple, efficient, and has the potential for vertical LIA measurements.	Empirical, and is affected by solar viewing geometry.	[71,72]

3. Remote Sensing Methods

Remote sensing methods provide large-scale and continuous LIA mapping based on empirical relationships, radiative transfer model inversion, and the gap fraction method [17–19,74].

3.1. Empirical Methods

MLA can be estimated empirically from canopy reflectance or vegetation indices by constructing a transfer function [75]. Zou and Mõttus [75] found that the near-infrared (NIR) reflectance, especially in the 748 nm in the red-edge band, showed a negative linear relationship with the crop MLA and the output MLA showed medium consistency with the reference MLA. They also showed that the MLA can be determined from the red and blue reflectance space, but the estimated MLA showed poor correspondence with the reference value [75]. Different LAD types can also be empirically distinguished. For example, Huang, Niu, Wang, Liu, Zhao, and Liu [17] identified different winter wheat LAD types from the multi-temporal NIR reflectance. In simulation studies, the backscattering coefficient of the microwave horizontal polarization was found to correlate to LAD [76], but no LIA inversion studies with microwaves have been reported.

The angular reflectance varies with MLAs and can assist the MLA estimation [77]. The angular reflectance is commonly described by the bidirectional reflectance distribution function (BRDF). One of the widely used BRDF models is the semi-empirical Ross-Li model, which characterizes the bidirectional reflectance with a linear combination of the volumetric, geometric, and isotropic kernels [78]. The structural parameter-sensitive index (SPEI) has been constructed from BRDF weights to identify the winter wheat LAD types [17].

$$\begin{cases} SPEI = OA/OAL \\ OA = f_{vol}^{nir} - \frac{f_{iso}^{nir}}{10} - f_{geo}^{red} \\ OAL = f_{vol}^{nir} + \frac{f_{iso}^{nir}}{10} - f_{geo}^{red} \end{cases} \quad (5)$$

where f_{iso}^{nir} and f_{vol}^{nir} are the weights of the isotropic and volumetric scattering kernels in the NIR band, respectively, and f_{geo}^{red} is the weight of the geometric scattering kernel in the red band [17,79].

The vegetation index (VI) has shown great potential to estimate MLA because of its simplicity and capability to mitigate the soil background effect [80,81]. Existing simulation studies have shown that the modified triangular vegetation index (MTVI2) [82] and two-band enhanced vegetation index (EVI2) [83] are strongly correlated negatively with MLA, especially for low and medium LAI (LAI < 3) [80].

$$MTVI2 = \frac{1.5\left[1.2\left(\rho_{NIR} - \rho_{green}\right) - 2.5\left(\rho_{red} - \rho_{green}\right)\right]}{\sqrt{\left(2\rho_{NIR} + 1\right)^2 - \left(6\rho_{NIR} - 5\sqrt{\rho_{red}}\right)^{-0.5}}} \quad (6)$$

$$EVI2 = 2.5(\rho_{NIR} - \rho_{red})/(\rho_{NIR} + 2.4\rho_{red} + 1) \quad (7)$$

where ρ_{NIR}, ρ_{red}, and ρ_{green} denote the NIR, red, and green reflectances, respectively.

The empirical method is easy to use, but it relies on a large number of field measurements, which limits the method's generality. Currently, the method has been applied to crops with medium accuracy [75]. The applicability of this method to noncrops needs to be further explored. The reflectance-based method is easily affected by LAI, leaf dry matter content, and soil background [77,81,84]. The method works better for the medium LAI conditions when the impacts of those factors are suppressed [77,81,84]. The angular reflectance has been used to distinguish different LAD types qualitatively [17] and is promising for estimating LIA quantitatively. The VI method suppresses the soil background and chlorophyll impact and more effort can be made to estimate LIA from VI in practice. Combining multiple vegetation indices may also help decouple LIA from the LAI and leaf dry matter impact.

3.2. Radiative Transfer Model Methods

Radiative transfer models link canopy reflectance with a series of leaf optical properties and canopy structural parameters (LAD, LAI, and CI) for different solar-viewing geometries [6,85,86]. The RTM method obtains an optimal solution that minimizes the cost function between the simulated and observed reflectance using the look-up table, numerical optimization, and machine learning technologies [87]. Currently, most LAD retrievals are based on the PROSAIL model which integrates the PROSPECT leaf spectral model [88] and the Scattering by Arbitrarily Inclined Leaves (SAIL) canopy bidirectional reflectance model [85].

Multi-angle reflectance is commonly used for LAD retrieval [18,77,89]. For example, Jacquemoud et al. [89] retrieved LAD from the ground and airborne multi-angle NIR reflectance based on the PROSAIL model but the result was not satisfactory, especially for canopies with high LAI and horizontal LAD. Ferreira et al. [90] inverted the individual crown LIA from the airborne imaging spectroscopy based on the discrete anisotropic radiative transfer (DART) model and look-up table method. The RTM method has also been applied to estimate the seasonal grassland MLA from the Landsat reflectance, but the result showed strong anomalous fluctuations [91]. Currently, the RTM method is only validated with field measurements in a direct point-to-pixel manner for crops [75,91].

The RTM method has mainly been applied in local regions, but the method is promising for large-scale LIA time series mapping. However, the method is affected by the different LAD settings in radiative transfer models (Bacour et al. [92]). The method is also affected by the ill-posed problem in the inversion process [18,90,91]. Several approaches have been proposed to improve LIA retrieval through regularization with prior information. One solution is to provide background characteristics in the RTM inversion, such as the VI-LAI empirical relationship, leaf spectral, soil reflectance, and skylight fraction [18,84]. The temporal constraint assumes that the seasonal variation of the LIA is negligible [84]. The object-based inversion strategy exerts spatial constraint on the inversion process by assuming that the LIAs of adjacent pixels are similar [19].

3.3. The Gap Fraction Method

The gap fraction method discussed in Section 2.2.1 can also be used to estimate the global leaf projection function (G) from remote sensing data [74]. For example, the global nadir leaf projection function $G(0)$ can be estimated based on the Beer–Lambert law (Equation (1)):

$$G(0) = -\frac{ln^{(1-FVC)}}{CI(0) * LAI} \approx -\frac{ln^{(1-FVC)}}{CI * LAI} \quad (8)$$

where the nadir gap fraction is calculated from the fractional vegetation cover ($P(0) = 1 - FVC$) and the nadir clumping index ($CI(0)$) is approximated by the whole CI [74]. However, this method to estimate G is limited by the accuracy and consistency of remote sensing products [93].

4. Prospects

4.1. LIA Field Measurement

A variety of field measurement methods have been proposed to measure LIA. However, there are several gaps in current LIA field measurement studies. Firstly, the amount and spatial distribution of LIA field measurements need to be expanded to improve the biome and spatial representativeness. The spatial distribution of LIA field measurements can be improved by incorporating the LIA measurements into existing ground observation networks, such as the National Ecological Observatory Network (NEON) [94], Integrated Carbon Observation System (ICOS) [95], and Terrestrial Ecosystem Research Network (TERN) [96]. The LIA can be obtained synchronously with other canopy structure parameters, such as LAI, CI, and FVC. Secondly, Continuous LIA observations are necessary to understand the LIA temporal variations [29,32,54], but currently, there are only a few

continuous measurements for crops [22,29,47]. Automated and continuous observation and processing systems provide a practical way for acquiring the temporal LIA [97–99]. Thirdly, azimuthal LIA variations are conducive to 3D scene construction and realizing accurate radiative transfer modeling [22,100], but azimuthal LIA measurements are scarce. LiDAR provides an efficient way to capture the azimuthal LIA. Finally, the vertical variation of LIA is required in the layered RTM [101,102], but the vertical LIA data are limited in current measurements and can be obtained through LDP and LiDAR measurements on a tower, lift, or UAV.

Advanced computer vision and deep learning methods may promote LIA field measurements. For example, object detection technologies can be introduced to identify the leaf edge and extract the needleleaf in photographic methods. This will automatize LIA computation and reduce manual involvement. The deep learning methods can be used for the DHP image classification to improve the classification accuracy [103,104]. In addition, different measuring schemes and data organizations were used in the currently published LIA dataset, while a standard measurement protocol is recommended in the future to enhance the utilization of the measurements [105–107].

4.2. Global LIA Mapping

Global LIA mapping is significant in understanding the LIA spatial patterns, biophysical variables retrieval, and land surface modeling, but no global LIA map is available currently. One method for global mapping is using a machine learning approach based on the LIA ground data [105,107] and other predictive variables. In global mapping, LIA can be regarded as a species-specific structural trait [32,34,108] and subtle variations within a species can be ignored [19,84]. In this case, the species geolocation information and the LIA data can be combined to increase the LIA spatial distribution. The cropland is highly affected by the planting pattern and the cropland LIA can be derived for each crop type based on the regularly updated crop maps [109,110].

The RTM-based inversion method (Section 3.2) has great potential for continuous LIA estimation on a large scale from multi-angular and multi-temporal reflectance provided by MODIS, POLDER, and MISR sensors. The Earth Polychromatic Imaging Camera (EPIC) instrument on the Deep Space Climate Observatory (DSCOVR) at the first Lagrange point provides unique viewing geometry from nearly hotspot directions [111], and the recently launched Chinese terrestrial ecosystem carbon monitoring satellite (Gou Mang) provides multi-angle data (0°, ±19°, ±41°) [112]. Both the EPIC and Gou Mang data can be used for LIA inversion. Considering the sensitivity of the estimated LIA to RTM used in inversion [93], developing advanced LIA inversion models suitable for different biomes is required. Regularization strategies with temporal-spatial constraints can be adopted within the inversion process to improve the temporal-spatial stability of the retrieved LIA [19,84].

In addition, current LIA remote sensing retrieval methods have been mainly tested in local regions and still need more validation with more reference data, particularly for forests [75,92]. During the validation, the LIA can be upscaled through a weighted averaging method with LAI or vegetation indices.

5. Conclusions

This study provides a comprehensive review of LIA field measurements and remote sensing estimation methods. The field methods can be grouped into direct and indirect methods. The direct methods, particularly with inclinometer, LDP, and LiDAR, are commonly used for LIA measurements at the individual leaf, crown, and plot levels. Both LDP and LiDAR are promising for obtaining the vertical LIA profiles using lifting platforms and UAVs, while LiDAR can also conveniently obtain the azimuthal LIA. The indirect methods are more suitable for determining the LIA for crops than for forests at the plot scale. It is recommended to incorporate LIA measurements into existing ground observation networks to improve LIA spatial coverage. Automated and continuous observation systems can be developed to facilitate temporal LIA acquisition.

The remote sensing estimation methods include the empirical, radiative transfer model, and gap fraction methods. The remote sensing methods have been tested in local regions and more validation studies are necessary for other areas. The RTM method has great potential for estimating seasonal LIA on a large scale, while the inversion strategy can be improved. Global LIA mapping can be realized through the gap-filling of ground measurements.

Currently, the LIA field measurements are still limited in spatial coverage, temporal continuity, and vertical and azimuthal variations, while large-scale remote sensing of LIA is lacking. More attention should be paid to LIA field measurements and remote sensing studies in the future.

Author Contributions: Conceptualization, S.L., H.F. and Y.Z.; writing—original draft preparation, S.L.; writing—review and editing, S.L., H.F. and Y.Z. All authors have read and agreed to the published version of the manuscript.

Funding: This work was mainly supported by the National Natural Science Foundation of China, grant number 42171358 (H.F.).

Acknowledgments: We thank the anonymous reviewers for their helpful insights in improving this paper.

Conflicts of Interest: The authors declare no conflict of interest.

References

1. Wilson, J. Inclined point quadrats. *New Phytol.* **1960**, *59*, 1–7. [CrossRef]
2. van Zanten, M.; Pons, T.L.; Janssen, J.A.M.; Voesenek, L.A.C.J.; Peeters, A.J.M. On the Relevance and Control of Leaf Angle. *Crit. Rev. Plant Sci.* **2010**, *29*, 300–316. [CrossRef]
3. Hikosaka, K.; Hirose, T. Leaf angle as a strategy for light competition: Optimal and evolutionarily stable light-extinction coefficient within a canopy. *Ecoscience* **1997**, *4*, 501–507. [CrossRef]
4. Mantilla-Perez, M.B.; Salas Fernandez, M.G. Differential manipulation of leaf angle throughout the canopy: Current status and prospects. *J. Exp. Bot.* **2017**, *68*, 5699–5717. [CrossRef] [PubMed]
5. Sellers, P.J. Canopy reflectance, photosynthesis and transpiration. *Int. J. Remote Sens.* **1985**, *6*, 1335–1372. [CrossRef]
6. Ross, J. *The Radiation Regime and Architecture of Plant Stands*; Springer Science & Business Media: Berlin, Germany, 1981.
7. Xiao, Q.; McPherson, E.G.; Ustin, S.L.; Grismer, M.E. A new approach to modeling tree rainfall interception. *J. Geophys. Res. Atmos.* **2000**, *105*, 29173–29188. [CrossRef]
8. Maes, W.; Steppe, K. Estimating evapotranspiration and drought stress with ground-based thermal remote sensing in agriculture: A review. *J. Exp. Bot.* **2012**, *63*, 4671–4712. [CrossRef]
9. Liu, L.X.; Xu, S.M.; Woo, K.C. Influence of leaf angle on photosynthesis and the xanthophyll cycle in the tropical tree species Acacia crassicarpa. *Tree Physiol.* **2003**, *23*, 1255–1261. [CrossRef]
10. de Wit, C.T. *Photosynthesis of Leaf Canopies*; Centre for Agricultural Publications and Documentation: Wageningen, The Netherlands, 1965.
11. Campbell, G. Derivation of an angle density function for canopies with ellipsoidal leaf angle distributions. *Agric. For. Meteorol.* **1990**, *49*, 173–176. [CrossRef]
12. Thomas, S.C.; Winner, W.E. A rotated ellipsoidal angle density function improves estimation of foliage inclination distributions in forest canopies. *Agric. For. Meteorol.* **2000**, *100*, 19–24. [CrossRef]
13. Goel, N.S.; Strebel, D.E. Simple Beta Distribution Representation of Leaf Orientation in Vegetation Canopies. *Agron. J.* **1984**, *76*, 800. [CrossRef]
14. Nilson, T. A theoretical analysis of the frequency of gaps in plant stands. *Agric. Meteorol.* **1971**, *8*, 25–38. [CrossRef]
15. Lang, A.R.G. Leaf orientation of a cotton plant. *Agric. Meteorol.* **1973**, *11*, 37–51. [CrossRef]
16. Ryu, Y.; Sonnentag, O.; Nilson, T.; Vargas, R.; Kobayashi, H.; Wenk, R.; Baldocchi, D.D. How to quantify tree leaf area index in an open savanna ecosystem: A multi-instrument and multi-model approach. *Agric. For. Meteorol.* **2010**, *150*, 63–76. [CrossRef]
17. Huang, W.; Niu, Z.; Wang, J.; Liu, L.; Zhao, C.; Liu, Q. Identifying crop leaf angle distribution based on two-temporal and bidirectional canopy reflectance. *IEEE Trans. Geosci. Remote Sens.* **2006**, *44*, 3601–3608. [CrossRef]
18. Goel, N.S.; Thompson, R.L. Inversion of vegetation canopy reflectance models for estimating agronomic variables. V. Estimation of leaf area index and average leaf angle using measured canopy reflectances. *Remote Sens. Environ.* **1984**, *16*, 69–85. [CrossRef]
19. Atzberger, C.; Richter, K. Spatially constrained inversion of radiative transfer models for improved LAI mapping from future Sentinel-2 imagery. *Remote Sens. Environ.* **2012**, *120*, 208–218. [CrossRef]
20. Shell, G.S.G.S.G.; Lang, A.R.G.R.G.; Sale, P.J.M.J.M. Quantitative measures of leaf orientation and heliotropic response in sunflower, bean, pepper and cucumber. *Agric. Meteorol.* **1974**, *13*, 25–37. [CrossRef]

21. Lugg, D.G.; Youngman, V.E.; Hinze, G. Leaf Azimuthal Orientation of Sorghum in Four Row Directions. *Agron. J.* **1981**, *73*, 497. [CrossRef]
22. Kimes, D.S.; Kirchner, J.A. Diurnal variations of vegetation canopy structure. *Int. J. Remote Sens.* **1983**, *4*, 257–271. [CrossRef]
23. Zou, X.; Mõttus, M.; Tammeorg, P.; Torres, C.L.; Takala, T.; Pisek, J.; Mäkelä, P.; Stoddard, F.L.; Pellikka, P. Photographic measurement of leaf angles in field crops. *Agric. For. Meteorol.* **2014**, *184*, 137–146. [CrossRef]
24. Utsugi, H. Angle distribution of foliage in individual Chamaecyparis obtusa canopies and effect of angle on diffuse light penetration. *Trees* **1999**, *14*, 1–9. [CrossRef]
25. Zou, J.; Zhong, P.; Hou, W.; Zuo, Y.; Leng, P. Estimating Needle and Shoot Inclination Angle Distributions and Projection Functions in Five Larix principis-rupprechtii Plots via Leveled Digital Camera Photography. *Forests* **2020**, *12*, 30. [CrossRef]
26. Lang, A.R.G. An instrument for measuring canopy structure. *Remote Sens. Rev.* **1990**, *5*, 61–71. [CrossRef]
27. Sinoquet, H.; Rivet, P. Measurement and visualization of the architecture of an adult tree based on a three-dimensional digitising device. *Trees* **1997**, *11*, 265. [CrossRef]
28. Thanisawanyangkura, S.; Sinoquet, H.; Rivet, P.; Cretenet, M.; Jallas, E. Leaf orientation and sunlit leaf area distribution in cotton. *Agric. For. Meteorol.* **1997**, *86*, 1–15. [CrossRef]
29. Biskup, B.; Scharr, H.; Schurr, U.; Rascher, U. A stereo imaging system for measuring structural parameters of plant canopies. *Plant Cell Environ.* **2007**, *30*, 1299–1308. [CrossRef]
30. Rakocevic, M.; Sinoquet, H.; Christophe, A.; Varlet-Grancher, C. Assessing the geometric structure of a white clover (*Trifolium repens* L.) canopy using 3-D digitising. *Ann. Bot.* **2000**, *86*, 519–526. [CrossRef]
31. Pisek, J.; Ryu, Y.; Alikas, K. Estimating leaf inclination and G-function from leveled digital camera photography in broadleaf canopies. *Trees* **2011**, *25*, 919–924. [CrossRef]
32. Raabe, K.; Pisek, J.; Sonnentag, O.; Annuk, K. Variations of leaf inclination angle distribution with height over the growing season and light exposure for eight broadleaf tree species. *Agric. For. Meteorol.* **2015**, *214–215*, 2–11. [CrossRef]
33. McNeil, B.E.; Pisek, J.; Lepisk, H.; Flamenco, E.A. Measuring leaf angle distribution in broadleaf canopies using UAVs. *Agric. For. Meteorol.* **2016**, *218–219*, 204–208. [CrossRef]
34. Toda, M.; Ishihara, M.I.; Doi, K.; Hara, T. Determination of species-specific leaf angle distribution and plant area index in a cool-temperate mixed forest from UAV and upward-pointing digital photography. *Agric. For. Meteorol.* **2022**, *325*, 109151. [CrossRef]
35. Vicari, M.B.; Pisek, J.; Disney, M. New estimates of leaf angle distribution from terrestrial LiDAR: Comparison with measured and modelled estimates from nine broadleaf tree species. *Agric. For. Meteorol.* **2019**, *264*, 322–333. [CrossRef]
36. Pisek, J.; Sonnentag, O.; Richardson, A.D.; Mõttus, M. Is the spherical leaf inclination angle distribution a valid assumption for temperate and boreal broadleaf tree species? *Agric. For. Meteorol.* **2013**, *169*, 186–194. [CrossRef]
37. Ivanov, N.; Boissard, P.; Chapron, M.; Andrieu, B. Computer stereo plotting for 3-D reconstruction of a maize canopy. *Agric. For. Meteorol.* **1995**, *75*, 85–102. [CrossRef]
38. Wang, H.; Zhang, W.; Zhou, G.; Yan, G.; Clinton, N. Image-based 3D corn reconstruction for retrieval of geometrical structural parameters. *Int. J. Remote Sens.* **2009**, *30*, 5505–5513. [CrossRef]
39. Frasson, R.P.d.M.; Krajewski, W.F. Three-dimensional digital model of a maize plant. *Agric. For. Meteorol.* **2010**, *150*, 478–488. [CrossRef]
40. Müller-Linow, M.; Pinto-Espinosa, F.; Scharr, H.; Rascher, U. The leaf angle distribution of natural plant populations: Assessing the canopy with a novel software tool. *Plant Methods* **2015**, *11*, 11. [CrossRef]
41. Qi, J.; Xie, D.; Li, L.; Zhang, W.; Mu, X.; Yan, G. Estimating Leaf Angle Distribution From Smartphone Photographs. *IEEE Geosci. Remote Sens. Lett.* **2019**, *16*, 1190–1194. [CrossRef]
42. Yan, G.; Jiang, H.; Luo, J.; Mu, X.; Li, F.; Qi, J.; Hu, R.; Xie, D.; Zhou, G. Quantitative Evaluation of Leaf Inclination Angle Distribution on Leaf Area Index Retrieval of Coniferous Canopies. *J. Remote Sens.* **2021**, *2021*, 2708904. [CrossRef]
43. Wang, Y.; Fang, H. Estimation of LAI with the LiDAR Technology: A Review. *Remote Sens.* **2020**, *12*, 3457. [CrossRef]
44. Zheng, G.; Moskal, L.M. Leaf orientation retrieval from terrestrial laser scanning (TLS) data. *IEEE Trans. Geosci. Remote Sens.* **2012**, *50*, 3970–3979. [CrossRef]
45. Bailey, B.N.; Mahaffee, W.F. Rapid measurement of the three-dimensional distribution of leaf orientation and the leaf angle probability density function using terrestrial LiDAR scanning. *Remote Sens. Environ.* **2017**, *194*, 63–76. [CrossRef]
46. Itakura, K.; Hosoi, F. Estimation of Leaf Inclination Angle in Three-Dimensional Plant Images Obtained from Lidar. *Remote Sens.* **2019**, *11*, 344. [CrossRef]
47. Su, W.; Huang, J.; Liu, D.; Zhang, M. Retrieving Corn Canopy Leaf Area Index from Multitemporal Landsat Imagery and Terrestrial LiDAR Data. *Remote Sens.* **2019**, *11*, 572. [CrossRef]
48. Wu, X.; Fan, W.; Du, H.; Ge, H.; Huang, F.; Xu, X. Estimating Crown Structure Parameters of Moso Bamboo: Leaf Area and Leaf Angle Distribution. *Forests* **2019**, *10*, 686. [CrossRef]
49. Kuusk, A. Leaf orientation measurement in a mixed hemiboreal broadleaf forest stand using terrestrial laser scanner. *Trees* **2020**, *34*, 371–380. [CrossRef]
50. Li, Y.; Su, Y.; Hu, T.; Xu, G.; Guo, Q. Retrieving 2-D Leaf Angle Distributions for Deciduous Trees from Terrestrial Laser Scanner Data. *IEEE Trans. Geosci. Remote Sens.* **2018**, *56*, 4945–4955. [CrossRef]

51. Hosoi, F.; Omasa, K. Estimating leaf inclination angle distribution of broad-leaved trees in each part of the canopies by a high-resolution portable scanning lidar. *J. Agric. Meteorol.* **2015**, *71*, 136–141. [CrossRef]
52. Stovall, A.E.L.; Masters, B.; Fatoyinbo, L.; Yang, X. TLSLeAF: Automatic leaf angle estimates from single-scan terrestrial laser scanning. *New Phytol.* **2021**, *232*, 1876–1892. [CrossRef]
53. Ma, L.; Zheng, G.; Eitel, J.U.H.; Magney, T.S.; Moskal, L.M. Retrieving forest canopy extinction coefficient from terrestrial and airborne lidar. *Agric. For. Meteorol.* **2017**, *236*, 1–21. [CrossRef]
54. Liu, J.; Skidmore, A.K.; Wang, T.; Zhu, X.; Premier, J.; Heurich, M.; Beudert, B.; Jones, S. Variation of leaf angle distribution quantified by terrestrial LiDAR in natural European beech forest. *ISPRS J. Photogramm. Remote Sens.* **2019**, *148*, 208–220. [CrossRef]
55. Zhu, X.; Skidmore, A.K.; Darvishzadeh, R.; Niemann, K.O.; Liu, J.; Shi, Y.; Wang, T. Foliar and woody materials discriminated using terrestrial LiDAR in a mixed natural forest. *Int. J. Appl. Earth Obs. Geoinf.* **2018**, *64*, 43–50. [CrossRef]
56. Lang, A.R.G. Leaf-area and average leaf angle from transmission of direct sunlight. *Aust. J. Bot.* **1986**, *34*, 349–355. [CrossRef]
57. Welles, J.M.; Norman, J.M. Instrument for Indirect Measurement of Canopy Architecture. *Agron. J.* **1991**, *83*, 818. [CrossRef]
58. Norman, J.M.; Campbell, G.S. Canopy structure. In *Plant Physiological Ecology: Field Methods and Instrumentation*; Pearcy, R.W., Ehleringer, J.R., Mooney, H.A., Rundel, P.W., Eds.; Springer: Dordrecht, The Netherlands, 1989; pp. 301–325.
59. Weiss, M.; Baret, F. CAN-EYE V6.4.91 User Manual. 2017. Available online: https://www6.paca.inrae.fr/can-eye/Documentation/Documentation (accessed on 1 September 2019).
60. Thimonier, A.; Sedivy, I.; Schleppi, P. Estimating leaf area index in different types of mature forest stands in Switzerland: A comparison of methods. *Eur. J. For. Res.* **2010**, *129*, 543–562. [CrossRef]
61. Schleppi, P.; Conedera, M.; Sedivy, I.; Thimonier, A. Correcting non-linearity and slope effects in the estimation of the leaf area index of forests from hemispherical photographs. *Agric. For. Meteorol.* **2007**, *144*, 236–242. [CrossRef]
62. Qu, Y.; Wang, Z.; Shang, J.; Liu, J.; Zou, J. Estimation of leaf area index using inclined smartphone camera. *Comput. Electron. Agric.* **2021**, *191*, 106514. [CrossRef]
63. Zhao, K.; García, M.; Liu, S.; Guo, Q.; Chen, G.; Zhang, X.; Zhou, Y.; Meng, X. Terrestrial lidar remote sensing of forests: Maximum likelihood estimates of canopy profile, leaf area index, and leaf angle distribution. *Agric. For. Meteorol.* **2015**, *209–210*, 100–113. [CrossRef]
64. Zheng, G.; Moskal, L.M. Spatial variability of terrestrial laser scanning based leaf area index. *Int. J. Appl. Earth Obs. Geoinf.* **2012**, *19*, 226–237. [CrossRef]
65. Lin, Y.; West, G. Retrieval of effective leaf area index (LAIe) and leaf area density (LAD) profile at individual tree level using high density multi-return airborne LiDAR. *Int. J. Appl. Earth Obs. Geoinf.* **2016**, *50*, 150–158. [CrossRef]
66. Liu, J.; Wang, T.; Skidmore, A.K.; Jones, S.; Heurich, M.; Beudert, B.; Premier, J. Comparison of terrestrial LiDAR and digital hemispherical photography for estimating leaf angle distribution in European broadleaf beech forests. *ISPRS J. Photogramm. Remote Sens.* **2019**, *158*, 76–89. [CrossRef]
67. Fang, H. Canopy clumping index (CI): A review of methods, characteristics, and applications. *Agric. For. Meteorol.* **2021**, *303*, 108374. [CrossRef]
68. Wagner, S.; Hagemeier, M. Method of segmentation affects leaf inclination angle estimation in hemispherical photography. *Agric. For. Meteorol.* **2006**, *139*, 12–24. [CrossRef]
69. Mu, X.; Hu, R.; Zeng, Y.; McVicar, T.R.; Ren, H.; Song, W.; Wang, Y.; Casa, R.; Qi, J.; Xie, D.; et al. Estimating structural parameters of agricultural crops from ground-based multi-angular digital images with a fractional model of sun and shade components. *Agric. For. Meteorol.* **2017**, *246*, 162–177. [CrossRef]
70. Casa, R.; Jones, H.G. LAI retrieval from multiangular image classification and inversion of a ray tracing model. *Remote Sens. Environ.* **2005**, *98*, 414–428. [CrossRef]
71. Yang, B.; Zhao, H.; Chen, W. Semi-empirical models for polarized reflectance of land surfaces: Intercomparison using space-borne POLDER measurements. *J. Quant. Spectrosc. Radiat. Transf.* **2017**, *202*, 13–20. [CrossRef]
72. Shibayama, M.; Watanabe, Y. Estimating the Mean Leaf Inclination Angle of Wheat Canopies Using Reflected Polarized Light. *Plant Prod. Sci.* **2007**, *10*, 329–342. [CrossRef]
73. Chen, J.M.; Black, T.A.; Adams, R.S. Evaluation of hemispherical photography for determining plant area index and geometry of a forest stand. *Agric. For. Meteorol.* **1991**, *56*, 129–143. [CrossRef]
74. Fang, H.; Li, S.; Zhang, Y.; Wei, S.; Wang, Y. New insights of global vegetation structural properties through an analysis of canopy clumping index, fractional vegetation cover, and leaf area index. *Sci. Remote Sens.* **2021**, *4*, 100027. [CrossRef]
75. Zou, X.; Mõttus, M. Retrieving crop leaf tilt angle from imaging spectroscopy data. *Agric. For. Meteorol.* **2015**, *205*, 73–82. [CrossRef]
76. Lang, R.H.; Saleh, H.A. Microwave Inversion of Leaf Area and Inclination Angle Distributions from Backscattered Data. *IEEE Trans. Geosci. Remote Sens.* **1985**, *GE-23*, 685–694. [CrossRef]
77. Jacquemoud, S.; Verhoef, W.; Baret, F.; Bacour, C.; Zarco-Tejada, P.J.; Asner, G.P.; François, C.; Ustin, S.L. PROSPECT+SAIL models: A review of use for vegetation characterization. *Remote Sens. Environ.* **2009**, *113*, S56–S66. [CrossRef]
78. Li, X.; Strahler, A.H. Geometric-Optical Bidirectional Reflectance Modeling of a Conifer Forest Canopy. *IEEE Trans. Geosci. Remote Sens.* **1986**, *GE-24*, 906–919. [CrossRef]
79. Gao, F.; Schaaf, C.B.; Strahler, A.H.; Jin, Y.; Li, X. Detecting vegetation structure using a kernel-based BRDF model. *Remote Sens. Environ.* **2003**, *86*, 198–205. [CrossRef]

80. Liu, J.; Pattey, E.; Jégo, G. Assessment of vegetation indices for regional crop green LAI estimation from Landsat images over multiple growing seasons. *Remote Sens. Environ.* **2012**, *123*, 347–358. [CrossRef]
81. Dong, T.; Liu, J.; Shang, J.; Qian, B.; Ma, B.; Kovacs, J.M.; Walters, D.; Jiao, X.; Geng, X.; Shi, Y. Assessment of red-edge vegetation indices for crop leaf area index estimation. *Remote Sens. Environ.* **2019**, *222*, 133–143. [CrossRef]
82. Haboudane, D.; Miller, J.R.; Pattey, E.; Zarco-Tejada, P.J.; Strachan, I.B. Hyperspectral vegetation indices and novel algorithms for predicting green LAI of crop canopies: Modeling and validation in the context of precision agriculture. *Remote Sens. Environ.* **2004**, *90*, 337–352. [CrossRef]
83. Jiang, Z.; Huete, A.R.; Didan, K.; Miura, T. Development of a two-band enhanced vegetation index without a blue band. *Remote Sens. Environ.* **2008**, *112*, 3833–3845. [CrossRef]
84. Houborg, R.; Soegaard, H.; Boegh, E. Combining vegetation index and model inversion methods for the extraction of key vegetation biophysical parameters using Terra and Aqua MODIS reflectance data. *Remote Sens. Environ.* **2007**, *106*, 39–58. [CrossRef]
85. Verhoef, W. Light scattering by leaf layers with application to canopy reflectance modeling: The SAIL model. *Remote Sens. Environ.* **1984**, *16*, 125–141. [CrossRef]
86. Liang, S. *Quantitative Remote Sensing of Land Surfaces*; John Wiley & Sons: Hoboken, NJ, USA, 2005; Volume 30.
87. Fang, H.; Baret, F.; Plummer, S.; Schaepman-Strub, G. An Overview of Global Leaf Area Index (LAI): Methods, Products, Validation, and Applications. *Rev. Geophys.* **2019**, *57*, 739–799. [CrossRef]
88. Jacquemoud, S.; Baret, F. PROSPECT: A model of leaf optical properties spectra. *Remote Sens. Environ.* **1990**, *34*, 75–91. [CrossRef]
89. Jacquemoud, S.; Flasse, S.; Verdebout, J.; Schmuck, G. Comparison of several optimization methods to extract canopy biophysical parameters-application to CAESAR data. In Proceedings of the 6th International Symposium Physical Measurements and Signatures in Remote Sensing, Val d'Isere, France, 17–24 January 1994; pp. 291–298.
90. Ferreira, M.P.; Féret, J.-B.; Grau, E.; Gastellu-Etchegorry, J.-P.; do Amaral, C.H.; Shimabukuro, Y.E.; de Souza Filho, C.R. Retrieving structural and chemical properties of individual tree crowns in a highly diverse tropical forest with 3D radiative transfer modeling and imaging spectroscopy. *Remote Sens. Environ.* **2018**, *211*, 276–291. [CrossRef]
91. Bayat, B.; van der Tol, C.; Verhoef, W. Integrating satellite optical and thermal infrared observations for improving daily ecosystem functioning estimations during a drought episode. *Remote Sens. Environ.* **2018**, *209*, 375–394. [CrossRef]
92. Bacour, C.; Jacquemoud, S.; Leroy, M.; Hautecœur, O.; Weiss, M.; Prévot, L.; Bruguier, N.; Chauki, H. Reliability of the estimation of vegetation characteristics by inversion of three canopy reflectance models on airborne POLDER data. *Agronomie* **2002**, *22*, 555–565. [CrossRef]
93. Li, S.; Fang, H.; Zhang, Y.; Wang, Y. Comprehensive evaluation of global CI, FVC, and LAI products and their relationships using high-resolution reference data. *Sci. Remote Sens.* **2022**, *6*, 100066. [CrossRef]
94. Kao, R.H.; Gibson, C.M.; Gallery, R.E.; Meier, C.L.; Barnett, D.T.; Docherty, K.M.; Blevins, K.K.; Travers, P.D.; Azuaje, E.; Springer, Y.P.; et al. NEON terrestrial field observations: Designing continental-scale, standardized sampling. *Ecosphere* **2012**, *3*, art115. [CrossRef]
95. Gielen, B.; Acosta, M.; Altimir, N.; Buchmann, N.; Cescatti, A.; Ceschia, E.; Fleck, S.; Hörtnagl, L.; Klumpp, K.; Kolari, P.; et al. Ancillary vegetation measurements at ICOS ecosystem stations. *Int. Agrophysics* **2018**, *32*, 645–664. [CrossRef]
96. Karan, M.; Liddell, M.; Prober, S.M.; Arndt, S.; Beringer, J.; Boer, M.; Cleverly, J.; Eamus, D.; Grace, P.; Van Gorsel, E.; et al. The Australian SuperSite Network: A continental, long-term terrestrial ecosystem observatory. *Sci. Total Environ.* **2016**, *568*, 1263–1274. [CrossRef]
97. Chen, Y.; Jiao, S.; Cheng, Y.; Wei, H.; Sun, L.; Sun, Y. LAI-NOS: An automatic network observation system for leaf area index based on hemispherical photography. *Agric. For. Meteorol.* **2022**, *322*, 108999. [CrossRef]
98. Chianucci, F.; Bajocco, S.; Ferrara, C. Continuous observations of forest canopy structure using low-cost digital camera traps. *Agric. For. Meteorol.* **2021**, *307*, 108516. [CrossRef]
99. Niu, X.; Fan, J.; Luo, R.; Fu, W.; Yuan, H.; Du, M. Continuous estimation of leaf area index and the woody-to-total area ratio of two deciduous shrub canopies using fisheye webcams in a semiarid loessial region of China. *Ecol. Indic.* **2021**, *125*, 107549. [CrossRef]
100. Strebel, D.E.; Goel, N.S.; Ranson, K.J. Two-Dimensional Leaf Orientation Distributions. *IEEE Trans. Geosci. Remote Sens.* **1985**, *GE-23*, 640–647. [CrossRef]
101. Yang, P.; Prikaziuk, E.; Verhoef, W.; van der Tol, C. SCOPE 2.0: A model to simulate vegetated land surface fluxes and satellite signals. *Geosci. Model Dev. Discuss.* **2020**, *2020*, 1–26. [CrossRef]
102. Kuusk, A. A two-layer canopy reflectance model. *J. Quant. Spectrosc. Radiat. Transf.* **2001**, *71*, 1–9. [CrossRef]
103. Li, K.; Huang, X.; Zhang, J.; Sun, Z.; Huang, J.; Sun, C.; Xie, Q.; Song, W. A new method for forest canopy hemispherical photography segmentation based on deep learning. *Forests* **2020**, *11*, 1366. [CrossRef]
104. Richards, J.A.; Richards, J.A. *Remote Sensing Digital Image Analysis*; Springer: Berlin/Heidelberg, Germany, 2022; Volume 5.
105. Chianucci, F.; Pisek, J.; Raabe, K.; Marchino, L.; Ferrara, C.; Corona, P. A dataset of leaf inclination angles for temperate and boreal broadleaf woody species. *Ann. For. Sci.* **2018**, *75*, 50. [CrossRef]
106. Hinojo-Hinojo, C.; Goulden, M. A compilation of canopy leaf inclination angle measurements across plant species and biome types. *Zenodo* **2020**, *8*, 599–609. [CrossRef]
107. Pisek, J.; Adamson, K. Dataset of leaf inclination angles for 71 different Eucalyptus species. *Data Brief* **2020**, *33*, 106391. [CrossRef]

108. Pisek, J.; Diaz-Pines, E.; Matteucci, G.; Noe, S.; Rebmann, C. On the leaf inclination angle distribution as a plant trait for the most abundant broadleaf tree species in Europe. *Agric. For. Meteorol.* **2022**, *323*, 109030. [CrossRef]
109. Boryan, C.; Yang, Z.; Mueller, R.; Craig, M. Monitoring US agriculture: The US department of agriculture, national agricultural statistics service, cropland data layer program. *Geocarto Int.* **2011**, *26*, 341–358. [CrossRef]
110. d'Andrimont, R.; Verhegghen, A.; Lemoine, G.; Kempeneers, P.; Meroni, M.; van der Velde, M. From parcel to continental scale—A first European crop type map based on Sentinel-1 and LUCAS Copernicus in-situ observations. *Remote Sens. Environ.* **2021**, *266*, 112708. [CrossRef]
111. Marshak, A.; Herman, J.; Szabo, A.; Blank, K.; Cede, A.; Carn, S.; Geogdzhayev, I.; Huang, D.; Huang, L.K.; Knyazikhin, Y.; et al. Earth Observations from DSCOVR/EPIC Instrument. *Bull. Am. Meteorol. Soc.* **2018**, *99*, 1829–1850. [CrossRef] [PubMed]
112. Li, G.; Gao, X.; Hu, F.; Guo, A.; Liu, Z.; Chen, J.; Liu, C.; Nie, S.; Fu, A. Overview of the Terrestrial Ecosystem Carbon Monitoring Satellite Laser Altimeter. *Int. Arch. Photogramm. Remote Sens. Spat. Inf. Sci.* **2022**, *43*, 53–58. [CrossRef]